2020 IEEE/RSJ International Conference on Intelligent Robots and Systems (IROS)
October 25-29, 2020, Las Vegas, NV, USA (Virtual)

PnuGrip: An Active Two-Phase Gripper for Dexterous Manipulation

Ian H. Taylor[1], Nikhil Chavan-Dafle[1], Godric Li[1], Neel Doshi[1,2], and Alberto Rodriguez[1]
<ihtaylor, nikhilcd, nddoshi, albertor>@mit.edu

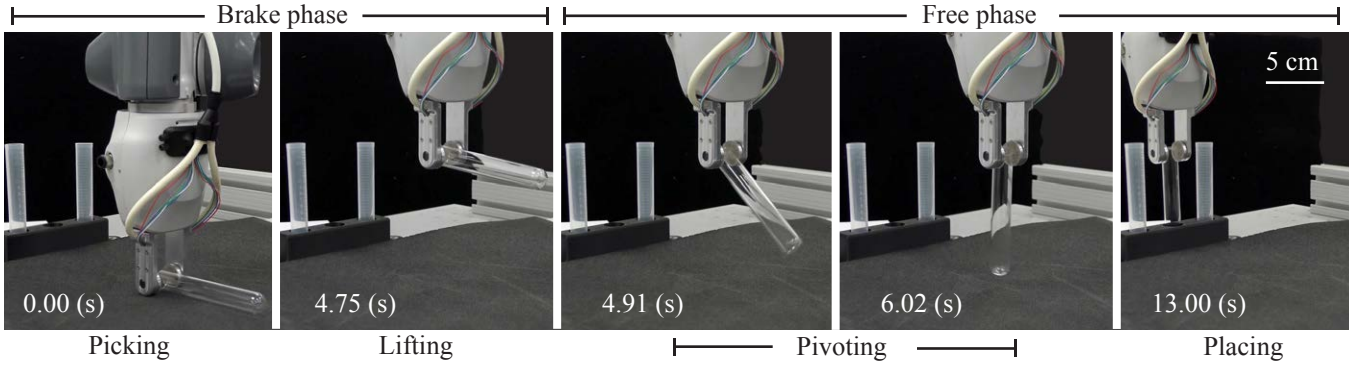

Fig. 1. Our active two-phase fingers mounted on a simple parallel-jaw gripper enable a dexterous pick-and-place task. The robot picks up a glass test-tube in the brake phase, and it then transitions to the free phase to reorient and place the test-tube vertically.

***Abstract*— We present the design of an *active* two-phase finger for mechanically mediated dexterous manipulation. The finger enables re-orientation of a grasped object by using a pneumatic braking mechanism to transition between free-rotating and fixed (i.e., braked) phases. Our design allows controlled high-bandwidth (5 Hz) phase transitions independent of the grasping force for manipulation of a variety of objects. Moreover, its thin profile (1 cm) facilitates picking and placing in clutter. Finally, the design features a sensor for measuring fingertip rotation to support feedback control. We experimentally characterize the finger's load handling capacity in the brake phase and rotational resistance in the free phase. We also demonstrate several pick-and-place manipulations common to industrial and laboratory automation settings that are simplified by our design.**

I. Introduction

Dexterous manipulation involves moving an object in hand, usually through contact interactions. Planning and controlling these interactions often boils down to planning contact locations and modes (e.g., sliding, sticking, rolling, pivoting) and maintaining them through control schemes. Enforcing a sequence of planned motions can be challenging under model uncertainty and with limited sensing. Task-driven hardware design, however, can simplify both planning and execution of dexterous manipulations.

This paper presents an *active* two-phase finger design that pneumatically enables mode transitions between a free rotating fingertip (free phase) and a stationary fingertip (brake phase). Our finger design presents three main features:

- **Active mode transitions** allow full control of transitions between the free rotation and brake phases of the fingertip independent of the grasping force.
- **The thin profile** of the finger allows access to and precise placement of objects in clutter.
- **High bandwidth control** that is made possible by fast transitions between the free and brake phases and a high-resolution encoder.

We describe the design of our active two-phase finger in Section III and Section IV. The fingertip is secured by a bearing to the body of the finger. A rubber diaphragm sits between the body and fingertip with a small clearance. When pressurized, the diaphragm inflates and presses against the back of the fingertip, "braking" the fingertip's free-rotation. Depressurising the diaphragm immediately releases the brake allowing free-rotation of the fingertip again. Since this transition is independent of the grasping force, it enables manipulation of objects that require different grasping forces (e.g., heavy or light, rigid or delicate).

We also validate the load handling capacity (braking capacity) of the two-phase fingers as a function of the applied air-pressure in Section V. Furthermore, our experiments verify that there is minimal rotational resistance in the free phase, allowing the fingertips to rotate irrespective of the applied grasping force. Finally, we observe that the transition between the free and brake phases takes a fraction of a second.

Finally, we use this two-phase finger to actively reorient objects in a parallel-jaw grasp for a few manually programmed pick-and-place operations; for example, picking up a glass test-tube off a table and placing it vertically in a stand (Fig. 1). This scenario highlights some of the aforementioned features of our finger, namely the ability to grasp and pivot

[1]Dept. of Mechanical Engineering, Massachusetts Institute of Technology
[2]Intelligence Community Postdoctoral Research Fellowship Program, Massachusetts Institute of Technology, Cambridge, MA

fragile objects and then place them in tight arrangements. We believe our active two-phase gripper enables opportunities for new planning methods that can exploit this controllable degree of freedom at the fingertips for complex manipulation tasks.

II. Related work

In this section, we review related work on designing hardware to control the contact mode (Sec. II-A) and its application to simplifying planning and control for manipulation primitives (Sec. II-B).

A. Design for controlling contact mode

In this work, we use a pneumatic brake to control the contact mode (i.e. sticking or rotating) between the gripper and the grasped object. We are inspired by prior work on the use of switchable adhesion, including electromagnetic, pneumatic, and electrostatic, to control contact mode in both manipulation and locomotion.

Adhesion is often used to maintain and release contact between the robot and its environment. In locomotion, this can be used to enable climbing; for example, Zhu et. al [1] and Kim et. al [2] use switchable suction in the design of tracked robots that can adhere to the inclined surface. Similarly, De Rivaz et. al [3] and Gu et. al [4] use electroadhesion to design insect-scale legged and soft climbers, respectively. In manipulation, suction cups can be used to make and release contact between the end-effector and the object. The success of this approach has made suction ubiquitous in the design of grippers for bin-picking tasks [5].

Switchable adhesion can also be used to facilitate transitions between sticking and sliding contact modes. For example, Becker et. al [6] use pneumatics to alter the frictional proprieties of a soft-gripper to switch between sticking and sliding contact. As described below, such mechanically mediated contact-transitions can be useful for dexterous manipulations.

B. Design for dexterous manipulation

Traditionally, researchers have developed methods for dexterous manipulation that plan robot motions based on models of the system's mechanics [7], [8], [9]. For fast and efficient planning, many recent approaches restrict these models to specific contact modes (e.g., only sticking or sliding) and achieve dexterous manipulation as a concatenation of simple rotational, translational, and precessional motions [10], [11], [12], [13]. The accuracy of the generated motions, however, depends on the knowledge of the physical parameters of the system, which are often difficult to estimate precisely.

On the other hand, addressing the need for dexterity with task-specific mechanical solutions is common in industry. Part feeders reorient and locate objects so robots can simply pick and place them [14]. Moreover, fixtures around robots help them re-grasp an object through a series of place-and-pick operations. Similarly, recent research looks into building grippers that facilitate dexterous manipulations. Chavan-Dafle et al. present the idea of two-phase gripper to pivot and grasp objects using gravity [15]. Spiers et al. design fingers with switchable friction pads to contact the grasped object as needed and reorient it in the grasp [16] for table-top manipulations.

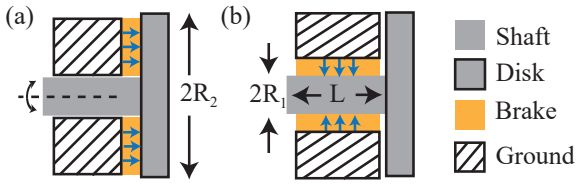

Fig. 2. A schematic showing two locations for applying braking pressure to the fingertip, the disk (a) or the shaft (b). The brake-torque generated by applying pressure at the disk is greater than that at the shaft for $R > L$.

Combining the merits of the two approaches described above, Hou et al. [17] and Terasaki and Hasegawa [18] present mechanisms and planners for object re-orientation. They design a gripper with free-rotating fingertips that can be made stationary with a grasping force higher than certain threshold. They then integrate this controllable finger rotation into their in-hand manipulation planner for increased dexterity. Their designs, however, require the transition threshold to be manually set beforehand for objects of different weights. In this paper, we focus on developing a similar two-phase gripper, but with an *active* phase transition that is independent of the grasping force. Our gripper can be used to manipulate a range of objects without prior tuning and adjustment.

III. Design requirements and selection

In this section, we describe the design requirements for our finger (Section III-A). Based on these requirements, we explore two candidate brake configurations (Section III-B), and three possible braking mechanisms (Section III-C).

A. Design requirements

The ability to seamlessly handle and reorient objects is particularly useful for electronics assembly and medical lab automation where objects need to be picked up and placed in tight arrangements. Typical objects in these applications are small and lightweight. Consequently, we assume the mass and half length of a typical object to be manipulated are $\leq$50 g and $\sim$5 cm, respectively. Under this estimate, with a factor of safety of 4$\times$, the maximum frictional torque required is 0.1 N m.

Based on our observations of grippers commonly used in industrial pick-and-place applications, we aim to have a fingertip with a diameter of about 2 cm. We also try to minimize the thickness of the finger to allow for grasping in clutter. Finally, we want to include the ability to measure the rotation of the fingertips for feedback and control applications.

B. Brake configuration

Our two-phase finger has two possible brake configurations: a disk-brake (Fig. 2a) and a shaft-brake (Fig. 2b). As per our design requirements, the finger needs to support a torque of 0.1 N m in the brake phase. The analysis presented here shows that, for our application, a larger brake-torque

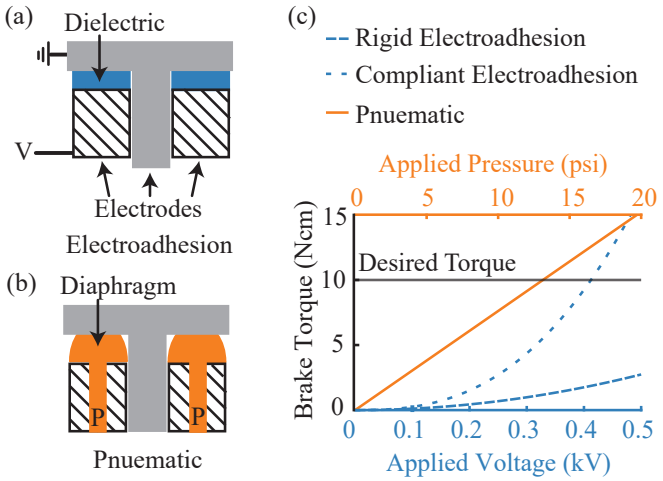

Fig. 3. Schematics showing an (a) electrostatic disk-brake and (b) a pneumatic disk-brake in the brake phase. (c) Brake-torque as a function of applied voltage (pressure) for the electrostatic (pneumatic) brakes. The desired torque is achieved at approximately 13 psi with a pneumatic brake and 410 V using a compliant electroadhesive brake.

can be generated using a disk-brake. Assuming a uniform pressure distribution, the brake-torque is computed as the product of the coefficient of friction between the brake and the fingertip (μ), the braking pressure (P), the contact area (A), and the distance between the centers of rotation and pressure (r_{eff}) [19]:

$$\tau_{\text{brake}} = \mu P A r_{\text{eff}}. \tag{1}$$

The brake torque for the disk-brake is then given by

$$\tau_{\text{disk}} = \mu P \pi (R_2^2 - R_1^2) \frac{R_2 + R_1}{2}, \tag{2}$$

where R_2 and R_1 are the outer and inner radii of the disk, respectively. The same for the shaft-brake is

$$\tau_{\text{shaft}} = 2\mu P \pi R_1 L R_1, \tag{3}$$

where L and R_1 are the length and radius of the shaft, respectively. We see that $\tau_{\text{disk}} \propto R^3$ and $\tau_{\text{shaft}} \propto R^2 L$ for some effective R. The ratio of the two is then proportional to

$$\frac{\tau_{\text{disk}}}{\tau_{\text{shaft}}} \propto \frac{R}{L}. \tag{4}$$

We assume that $R > L$ as our design objective is to minimize the thickness of the gripper. In our implementation, $L \approx R_1$ and $R_2 \approx 4R_1$. Consequently, the torque generated by the disk-brake is approximately $10\times$ larger than the torque generated by the shaft-brake for the same applied pressure.

C. Braking mechanism

We now investigate different disk-braking mechanisms. In particular, we discuss rigid electrostatic (Fig. 3a), compliant electrostatic, and pneumatic (Fig. 3b) brakes. We evaluate each mechanism based on its torque generation capability (Fig. 3c) and present our rationale for using pneumatic braking. We note that the analysis presented here is simplified and neglects implementation-specific details to allow a fair comparison between the braking mechanisms.

1) Rigid electrostatic brake: An electrostatic brake (Fig. 3a) consists of a dielectric material (blue) that is attached to the finger-body (striped) and barely touches the fingertip (gray). In the brake phase, the finger-body is charged to a positive voltage (V) and the fingertip is grounded. Assuming both the finger-body and fingertip are made from conductive materials, the electrostatic pressure (P_{re}) between the two is given by [20]:

$$P_{\text{re}} = \varepsilon_d \varepsilon_0 \frac{V^2}{2t^2}, \tag{5}$$

where ε_0 is permittivity of vacuum and ε_d and t are the dielectric constant and thickness of the dielectric, respectively. Assuming a Coulomb friction model, the brake-torque is computed by combining (2) and (5):

$$\tau_{\text{re}} = \mu P_{\text{re}} A r_{\text{eff}} = \mu \pi (R_2^2 - R_1^2) P_{\text{re}} \frac{R_2 + R_1}{2}. \tag{6}$$

Here μ is the coefficient of friction between the fingertip and the dielectric material.

2) Compliant electrostatic brake: Recently, Diller et. al conducted an empirical design study on the electrostatic friction force (F_{ce}) between two compliant, conductive, rectangular electrodes separated by a dielectric [21]. They found that the Coulomb friction model (6) underestimates friction force by $\sim 10\times$, and instead proposed the following empirical relationship:

$$F_{\text{ce}} = \exp(c_1)\, l^{c_2}\, w^{c_3}\, t_d^{c_4}\, t_e^{c_5}\, V^{c_6}\, age^{c_7}. \tag{7}$$

Here l, w, and t_e are the length, width, and thickness of a single electrode, t_d is the thickness of the dielectric, and age is the age of the clutch in days. The fit coefficients, taken from Diller et. al, are $c_1 = -23.18$, $c_2 = 0.91$, $c_3 = 1.11$, $c_4 = -1.50$, $c_5 = -0.36$, $c_6 = 2.61$, and $c_7 = 0.29$.

Since $c_2 \approx c_3 \approx 1.0$, we can replace $l^{c_2} w^{c_3}$ with A in (7) and write the electrostatic pressure between two compliant electrodes as

$$P_{\text{ce}} = \frac{F_{\text{ce}}}{A} = \exp(c_1)\, t_d^{c_4}\, t_e^{c_5}\, V^{c_6}\, age^{c_7}. \tag{8}$$

Assuming we can incorporate compliant electrodes into a finger design, we treat (8) as a "best-case" scenario for the electrostatic brake. Assuming a uniform pressure distribution between the electrodes, the brake-torque is

$$\tau_{\text{ce}} = \mu \pi (R_2^2 - R_1^2) P_{\text{ce}} \frac{R_2 + R_1}{2}. \tag{9}$$

3) Pneumatic brake: The braking pressure for a pneumatic brake is equal to the pressure in the pneumatic line (P_l), and the brake-torque can be computed via (2):

$$\tau_{\text{pnu}} = \mu \pi (R_2^2 - R_1^2) P_l \frac{R_2 + R_1}{2}. \tag{10}$$

4) Mechanism comparison: We evaluate the three mechanisms in Fig. 3c. The geometric parameters are set to describe the maximum theoretical contact area: $R_1 = 2.5$ mm and $R_2 = 10$ mm. The coefficient of friction is $\mu = 0.6$ as in Diller et. al. As in our previous work [3], we assume the dielectric for the rigid electrostatic brake is a 12.5 µm

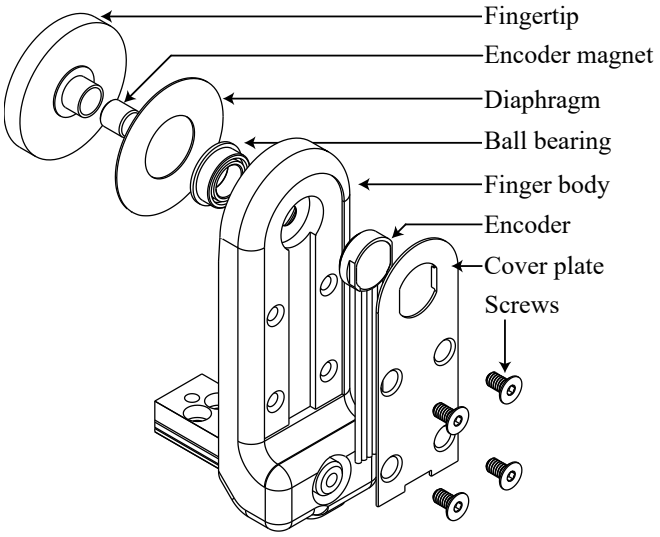

Fig. 4. Exploded line diagram of the computer-aided-design (CAD) model of our two-phase finger with individual components labelled.

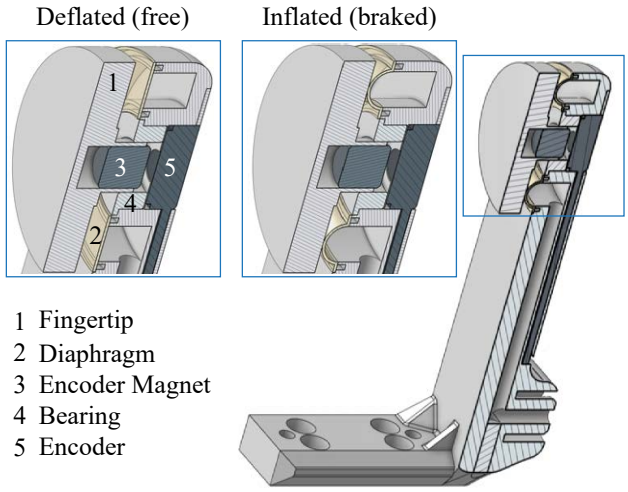

Fig. 5. A cross-sectional view of our two-phase finger (right). Enlarged cross-sections views of the distal end of the finger show the geometry of the diaphragm during the free phase (top-left) and the brake phase (top-middle). The gap between the fingertip and finger-body is enlarged in this figure for illustrative purposes.

thick polyimide sheet (Kapton, Dupont) as it has a high electrical breakdown voltage. This material has $\varepsilon_d = 3.5$ [22]. The parameters of the compliant electrostatic brake are t_e =20 µm, t_d =60 µm, and age =1 d. The thicknesses (t_e and t_d) are chosen to maximize the friction force based on Diller's model and the age is set to one for same-day use.

We find that the desired torque is achieved at ∼960 V using a rigid electrostatic brake, ∼410 V using a compliant electrostatic brake, and ∼13 psi using a pneumatic brake. We select a pneumatic configuration since a 13 psi pressure source is readily available while both electrostatic configurations require high voltages, and consequently, careful insulation.

IV. Design of Pneumatic Two-Phase Gripper

Here we give a more detailed description of the design of a two-phase finger (Section IV-A) and describe the assembly procedure (Section IV-B).

A. Design description

Fig. 4 shows the components of our two-phase finger. The fingertip, finger-body, and cover plate were custom machined out of aluminum (T6-6061) for precision and leak prevention. The body of the finger additionally accommodates a 2 mm diameter internal pneumatic routing line as well as the housing for a rotary encoder assembly (RLS, RM08 rotary encoder). The encoder magnet is placed within the axle of the fingertip and the fingertip is mounted in the finger-body with a precision fanged ball bearing. The finger is 1 cm thick at its tip, which is sufficiently thin for operation in cluttered scenarios. We chose an abrasion resistant 0.25 mm thick natural rubber as the diaphragm material for its low profile, elasticity, and tensile strength.

B. Finger assembly

First, the diaphragm was precision cut out of natural rubber sheet using a laser cutter. The bearing was press fit into the finger-body using a vice. Next, the finger-body was secured face-up in a vice and adhesive (Permabond Low Viscosity Instant Adhesive 910) was added to the two diaphragm bonding channels. Once both channels were filled the diaphragm was placed using tweezers and locating features on the finger-body to ensure proper alignment. Fig. 5 shows the shape of the diaphragm in deflated and inflated state and relative arrangement of the components near the distal end of the finger.

Next, the encoder magnet was inserted into the hollow axle of the fingertip and glued (Permabond 910) in place. The two assemblies were then left overnight to fully cure. Once the assemblies cured, the finger-body assembly was pressure tested to ensure proper bonding of the diaphragm. The fingertip and finger-body assemblies were then press fitted together using a vice. Finally the encoder was slotted in place at the back of the finger-body and the cover plate was attached using four M2 screws.

V. Experimental results and demonstrations

Here we describe the experimental setup (Section V-A) and procedures (Section V-B) used to characterize the performance of our two-phase finger. We present the results of these experiments in Section V-C and show a few demonstrations that highlight of our finger's capabilities in Section V-D.

A. Experimental setup

We performed an experimental characterization of our two-phase finger for three performance measures: (a) holding torque in the brake phase as a function of supplied pressure, (b) diaphragm void time as a function of supplied pressure, and (c) rotational resistance in the free phase as a function of grasp force. All three sets of experiments used the same experimental setup (Fig. 6) described below.

We mounted two of our two-phase fingers on a ABB Yumi robot's parallel-jaw gripper. We used a torque gauge

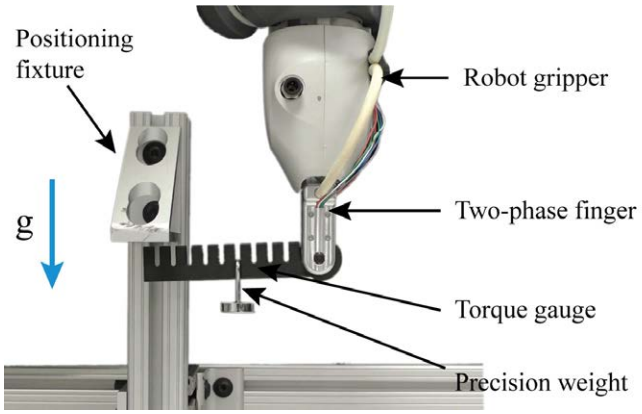

Fig. 6. Our active two-phase fingers are mounted on a ABB YuMi robot gripper. The torque gauge allows us to add external load and observe the brake-torque response of the fingers.

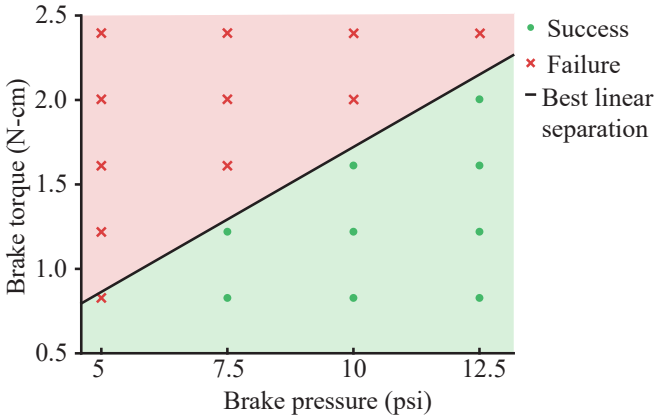

Fig. 7. Brake torque as a function of supplied pressure. Successful and failed trials are shown in green and red, respectively. We also show the best linear approximation to the separation boundary in black.

(weighing 9 g) with notches for holding precision weights at intervals of 1 cm. The gauge was firmly attached to both fingertips to prevent slip between the fingertips and the gauge during the experiments. A positioning-fixture was used to ensure that the initial angle of the gauge was consistent across all experiments.

The inflation of the diaphragm was controlled using a solenoid valve triggered by 24 V digital I/O signal from the YuMi Robot controller. The supplied pressure was varied via a manual air regulator between different experiments. Encoder data was collected from one of the fingers using the RLS E201 encoder interface. The experimental procedure was automated to trigger the pneumatic actuation and collect the encoder readings with their respective time-stamps.

B. Experimental procedure

We measure the frictional torque in the brake phase to validate the linear model described in Section III-C. Since the model has only one parameter, we measure brake torque for four supplied pressure values evenly spaced between 2.5 psi to 12.5 psi. For each pressure, the finger was loaded with a 20 g weight at five equally spaced distances between 2 cm to 10 cm. The gauge was then held against the positioning fixture to set the initial angle and the diaphragm was inflated, braking the fingertip. We then released the gauge and used the encoder data to record its final angle. The trials for which the gauge's rotation was less than 5° were considered successful. This threshold was set to accommodate the change in angle due to small shear deformations in the diaphragm that occurred at lower brake pressures.

A similar procedure to that previously described was used to characterize the time required for deflating the diaphragm (void time) as a function of the supplied pressure. For these experiments, the same four pressure values were used with no additional weight on the torque gauge. We conducted three trials for each supplied pressure. The void time was measured as the time between when brake was released by digital trigger and when the encoder measured that the gauge had rotated by 45°. The 45° angle was selected as a conservative estimate that the diaphragm had completely deflated.

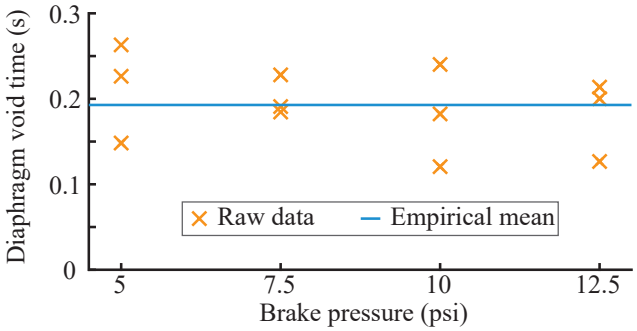

Fig. 8. Diaphragm void time in free phase as a function of brake pressure. The void time remains around 0.2 s independent of brake pressure. Raw-data and a line through the mean value is shown as an orange 'x' and a blue line, respectively.

Finally, we evaluate the rotational resistance in the free phase as a function of grasp force. For these experiments, four grasp force values were chosen in increments of 5 N from 5 N to 20 N. No additional weights were added to the gauge to test for the minimum loading case. We visually observed that in the free phase, the gauge rotates freely in the grasp irrespective of the grasping force.

C. Experimental results

The holding torque as a function of supplied pressure is shown in Fig. 7. The trials where the two-phase gripper was able to hold the applied torque are shown in green and the trials where the gripper failed are shown in red. The black line is the best linear (zero y-intercept) approximation to the boundary between the two regions. Since we are grasping with two fingers, the slope of this line, equal to $2\mu A r_{\text{eff}}$ (1), should be 1.5 Ncm/psi based on (10). As observed in Fig. 7, experimentally it is 0.17 Ncm/psi, approximately 9× smaller. This could be due to differences between the predicted and true coefficient of friction, contact area, and brake pressure. For example, the contact area between the diaphragm and the fingertip is likely much less than the maximum available area used for the calculations in Section III-C. If we assume the cross-section of the inflated diaphragm is a toroid, then the predicted contact area based on the geometry of the physical finger is about three times lesser.

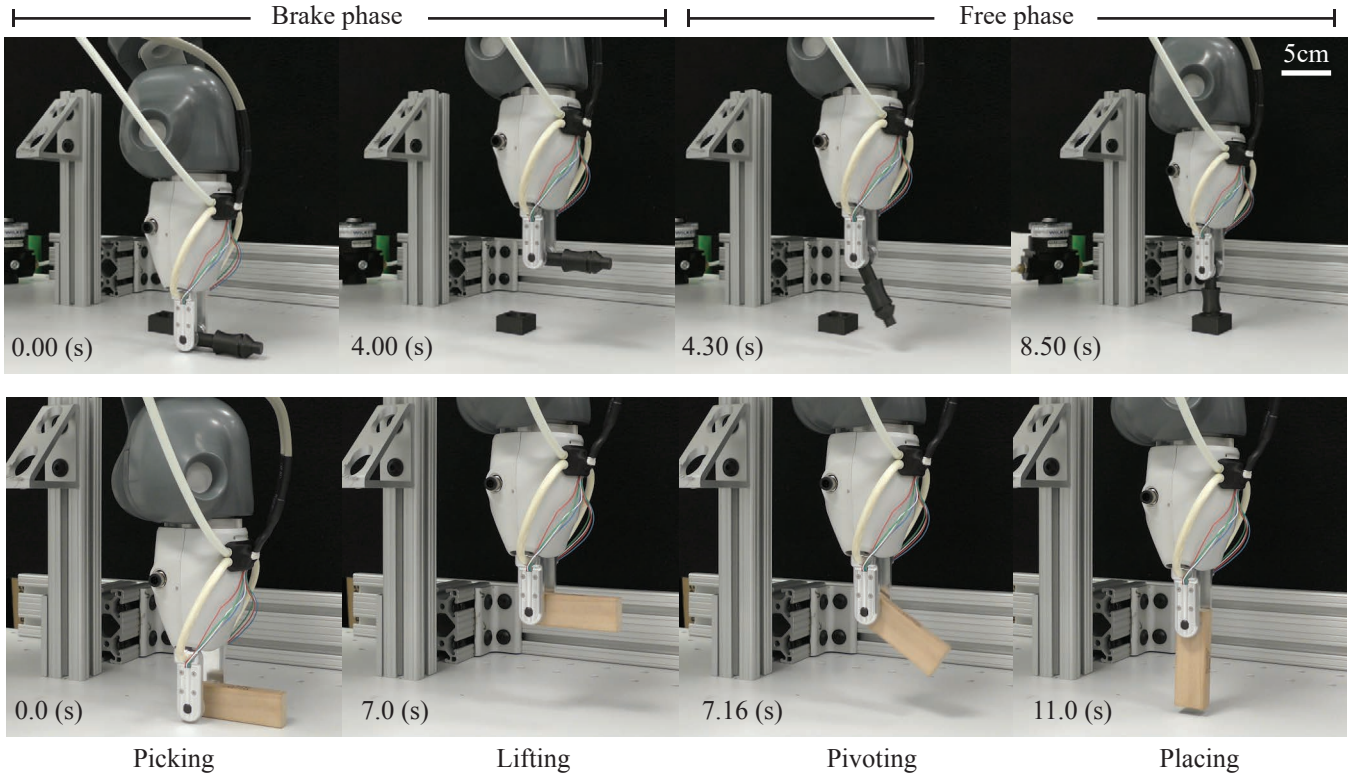

Fig. 9. Time-stamped images of our two-phase gripper picking, lifting, pivoting, and placing a cylindrical object of mass 7.2 g (top) and prismatic object of mass 15.2 g (bottom).

In the second set of experiments, we observed that the void time is almost constant for different brake pressures and is approximately 0.2 s as seen in Fig. 8. Given that the diaphragm can be inflated almost instantaneously, we can toggle between the free and brake phases at about 5 Hz.

D. Demonstrations

We highlight the utility of our active two-phase gripper in a number of manually scripted demonstrations. The first is a simple "lab-automation" task, shown in both Fig. 1 and the supplementary video. The robot picks up a glass test-tube (mass = 7.5 g, length = 10 cm) off a table in the brake phase, it then transitions to the free phase, as a result, the test-tube rotates 90° to align with the direction of gravity. Finally, the robot places the test-tube in a rack. Our fingers enable this task as they can grasp the test-tube with low-force to prevent damage and then exert the brake-force required to hold the tube at a desired angle. The low rotational friction in the free phase enables pivoting of this fairly light object, and the thin profile of the fingers allows for placement of a test-tube between two tightly arranged tubes.

We also conduct a similar pick-pivot-place experiment with a cylindrical object (mass = 7.2 g, length = 7.5 cm) in peg-in-hole setting. Finally, we perform a simple pick-pivot-place experiment with a heavier prismatic object (mass = (15.2 g) , length = 7.5 cm). These experiments, shown in Fig. 9 and in the supplementary video, demonstrate that we can grasp, hold, and rotate objects with different shapes and weight with no tuning of the gripper needed in between.

VI. Conclusion

We present the design of a novel two-phase finger with an active pneumatic brake. We analyze several brake configurations and mechanisms and select a pneumatic disk-brake since it both satisfies our design requirements and relies on a readily available power source. We also experimentally evaluate the performance of our gripper and observe that it can support a torque of about 0.02 N m at 12.5 psi in the brake phase, while grasped objects can freely rotate independent of grasp force in the free phase. We also note that void time remains constant across different supplied pressures.

Our gripper has several advantages over previous designs [15], [17], [23]. The most important is the ability to transition between the free and brake phases independent of the grasping force. Other advantages include a compact and simple design to enable grasping in clutter, an encoder to estimate the rotation of the grasped object, and quick and repeatable actuation.

A. Limitations

Our finger design prototyping and experimental testing has revealed a few limitations. One limitation of the current design relates to the lifespan of the gripper. The fingertip is currently secured by a single bearing, which makes it susceptible to orthogonal torques and reduces the lifespan of the bearing. Similarly, the rubber diaphragm directly contacts the fingertip during braking. This interaction will cause the diaphragm to wear, limiting its lifespan. The effects of these

limitations, however, can be evaluated via fatigue testing and the design can be modified (e.g., by placing a brake-pad over the diaphragm to protect it).

Moreover, mechanical imperfections in fabrication cause deviations from the theoretically expected braking performance. We will both characterize the effect of these imperfections on the brake torque and improve our design to limit their impact. Finally, the bandwidth of the pneumatic brake is currently limited to 5 Hz by the inflation/deflation time of the diaphragm. Though this is sufficient for simple pick and place manipulations, it could be improved by implementing an active suction mechanism to expedite the deflation.

B. Future work

We anticipate our future work to follow a few directions. The first is developing feedback strategies that utilize the encoder readings. We can potentially use the encoder readings from two fingers to estimate both the pose of the grasped object and and contact states (i.e., sticking or sliding) at the fingertips. A controller could then regulate both by modulating the brake torque and gripper pose. We can also develop planners that leverage the mechanically enabled reorientation capability of our gripper to decouple translational and rotational re-grasp planning [13] for complex and general dexterous manipulation.

VII. Acknowledgment

This research was partially supported by an appointment to the Intelligence Community Postdoctoral Research Fellowship Program at the Massachusetts Institute of Technology, administered by Oak Ridge Institute for Science and Education through an interagency agreement between the U.S. Department of Energy and the Office of the Director of National Intelligence.

References

[1] J. Zhu, D. Sun, and S. Tso, "Development of a tracked climbing robot," *Journal of Intelligent and Robotic Systems*, 2002.

[2] H. Kim, D. Kim, H. Yang, K. Lee, K. Seo, D. Chang, and J. Kim, "Development of a wall-climbing robot using a tracked wheel mechanism," *Journal of Mechanical Science and Technology*, pp. 1490–1498, 2008.

[3] S. D. de Rivaz, B. Goldberg, N. Doshi, K. Jayaram, J. Zhou, and R. J. Wood, "Inverted and vertical climbing of a quadrupedal microrobot using electroadhesion," *Science Robotics*, vol. 3, no. 25, 2018.

[4] G. Gu, J. Zou, R. Zhao, X. Zhao, and X. Zhu, "Soft wall-climbing robots," *Science Robotics*, vol. 3, no. 25, 2018.

[5] N. Correll, K. Bekris, D. Berenson, O. Brock, A. Causo, K. Hauser, K. Okada, A. Rodriguez, J. Romano, and P. Wurman, "Analysis and observations from the first amazon picking challenge," *T-ASE*, pp. 172–188, 2016.

[6] K. P. Becker, N. W. Bartlett, M. J. D. Malley, P. M. Kjeer, and R. J. Wood, "Tunable friction through constrained inflation of an elastomeric membrane," in *2017 IEEE International Conference on Robotics and Automation (ICRA)*. IEEE, 2017, pp. 4352–4357.

[7] J. Trinkle and R. Paul, "Planning for Dexterous Manipulation with Sliding Contacts," *Int J of Robot Res.*, vol. 9, no. 3, pp. 24–48, 1990.

[8] M. Cherif and K. Gupta, "Planning quasi-static fingertip manipulations for reconfiguring objects," in *IEEE T Robotic Autom*, vol. 15, 1999, pp. 837–848.

[9] D. Rus, "In-Hand Dexterous Manipulation of Piecewise-Smooth 3-D Objects," *Int J Robot Res*, vol. 18, no. 4, pp. 355–381, 1999.

[10] N. Chavan-Dafle, R. Holladay, and A. Rodriguez, "In-hand manipulation via motion cones," in *Robotics: Science and Systems (RSS)*, 2018.

[11] B. Sundaralingam and T. Hermans, "Relaxed-Rigidity Constraints: In-Grasp Manipulation using Purely Kinematic Trajectory Optimization," in *Proceedings of Robotics: Science and Systems*, 2017.

[12] S. Cruciani, C. Smith, D. Kragic, and K. Hang, "Dexterous manipulation graphs," *arXiv*, vol. abs/1803.00346, 2018.

[13] S. Cruciani, K. Hang, C. Smith, and D. Kragic, "Dual-arm in-hand manipulation and regrasping using dexterous manipulation graphs," *arXiv*, 2019.

[14] G. Monkman, S. Hesse, R. Steinmann, and H. Schunk, *Robot grippers*. John Wiley and Sons, 2006.

[15] N. Chavan-Dafle, M. T. Mason, H. Staab, G. Rossano, and A. Rodriguez, "A two-phase gripper to reorient and grasp," in *2015 IEEE International Conference on Automation Science and Engineering (CASE)*, Aug 2015, pp. 1249–1255.

[16] A. J. Spiers, B. Calli, and A. M. Dollar, "Variable-friction finger surfaces to enable within-hand manipulation via gripping and sliding," *IEEE Robotics and Automation Letters*, vol. 3, no. 4, pp. 4116–4123, Oct 2018.

[17] Y. Hou, Z. Jia, and M. T. Mason, "Fast planning for 3d any-pose-reorienting using pivoting," in *2018 IEEE International Conference on Robotics and Automation (ICRA)*. IEEE, 2018, pp. 1631–1638.

[18] H. Terasaki and T. Hasegawa, "Motion planning of intelligent manipulation by a parallel two-fingered gripper equipped with a simple rotating mechanism," vol. 14, no. 2, pp. 207–219, Apr 1998.

[19] U. C. Jindal, *Machine design*. Pearson Education India, 2010.

[20] K. H. Koh, R. M. Kuppan Chetty, and S. G. Ponnambalam, "Modeling and simulation of electrostatic adhesion for wall climbing robot," in *2011 IEEE International Conference on Robotics and Biomimetics*, 2011, pp. 2031–2036.

[21] S. B. Diller, S. H. Collins, and C. Majidi, "The effects of electroadhesive clutch design parameters on performance characteristics," *Journal of Intelligent Material Systems and Structures*, vol. 29, no. 19, pp. 3804–3828, 2018.

[22] *Kapton HN polyimide film Datasheet*, DuPont, 2011.

[23] H. Terasaki and T. Hasegawa, "Motion planning of intelligent manipulation by a parallel two-fingered gripper equipped with a simple rotating mechanism," *IEEE Transactions on Robotics and Automation*, vol. 14, no. 2, pp. 207–219, April 1998.